Neurobiology of Disease 40 (2010) 311–324

Contents lists available at ScienceDirect

Neurobiology of Disease

journal homepage: www.elsevier.com/locate/ynbdi

Polyglutamine toxicity induces rod photoreceptor division, morphological transformation or death in Spinocerebellar ataxia 7 mouse retina

Marina G. Yefimova [a,d], Nadia Messaddeq [a], Alice Karam [a], Carine Jacquard [a], Chantal Weber [a], Laurent Jonet [c], Uwe Wolfrum [b], Jean-Claude Jeanny [c], Yvon Trottier [a,*]

[a] Department of Neurobiology and Genetics, Institute of Genetics and Molecular and Cellular Biology (IGBMC), UMR 7104-CNRS/INSERM/UdS, BP10142, 67404 Illkirch Cédex, France
[b] Johannes Gutenberg University of Mainz, D-55099 Mainz, Germany
[c] Inserm UMRS 872 Team 17, Centre de Recherche des Cordeliers, Paris, France
[d] Sechenov Institute of Evolutionary Physiology and Biochemistry, Russian Academy of Sciences, 194223, St-Petersburg, Russia

ARTICLE INFO

Article history:
Received 15 March 2010
Revised 3 June 2010
Accepted 11 June 2010
Available online 18 June 2010

Keywords:
Polyglutamine
Neurodegeneration
Spinocerebellar ataxia 7
Photoreceptor
Proliferation
Remodeling
Retina
Toxicity
Dark neuronal death
Aggregate

ABSTRACT

In neurodegenerative disorders caused by polyglutamine (polyQ) expansion, polyQ toxicity is thought to trigger a linear cascade of successive degenerative events leading to neuronal death. To understand how neurons cope with polyQ toxicity, we studied a Spinocerebellar ataxia 7 (SCA7) mouse which expresses polyQ-expanded ATXN7 only in rod photoreceptors. We show that in response to polyQ toxicity, SCA7 rods go through a range of radically different cell fates, including apoptotic and non-apoptotic cell death, cell migration, morphological transformation into a round cell or, most remarkably, cell division. The temporal profile of retinal remodeling indicates that some degenerative pathways are triggered early in the disease but decline later on, while others worsen progressively. Retinal remodeling results in a relative maintenance of photoreceptor population, but does not preserve the retinal function. Rod responses to proteotoxicity correlate with the nature, level and ratio of mutant ATXN7 species. The multifaceted response of neurons to polyQ toxicity is an important concept for the design of therapeutic strategies.

Introduction

Spinocerebellar ataxia type 7 (SCA7) belongs to a group of nine inherited neurodegenerative disorders, including Huntington's disease (HD), that are caused by the expansion of CAG trinucleotide repeats encoding a polyglutamine (polyQ) tract in the corresponding disease proteins (Zoghbi and Orr, 2000). PolyQ expansion confers to mutant proteins toxic properties which are thought to rely on aberrant interaction of full-length mutant protein or its proteolytic fragments with natural protein partners, and on aggregation of polyQ fragments under diverse supramolecular forms (Williams and Paulson, 2008). These multiple toxic species gradually perturbs diverse cellular pathways that are essential for neuronal function and survival. How neurons cope with cumulative stresses induced by polyQ toxicity remains largely unclear.

SCA7 has a unique feature among polyQ diseases to cause a retinal degeneration (David et al., 1997). Patients first suffer from central vision deficit, which evolves toward complete blindness. Degenerative changes in the retina initially affect cone photoreceptors, and progress toward a cone-rod dystrophy (Michalik et al., 2004). Mouse models recapitulating the SCA7 retinal dystrophy display a progressive reduction of photoreceptor electroretinograph (ERG) function, without extensive loss of photoreceptor cells (La Spada et al., 2001; Yoo et al., 2003; Yvert et al., 2000). The SCA7 R7E transgenic mouse expresses the human ataxin-7 (ATXN7) with a polyQ expansion (90Q) under rhodopsin promoter control and thereby targets the expression in rod photoreceptors only (Yvert et al., 2000). Since lifespan is normal, R7E mouse allows the study of short and long term pathogenic effects of polyQ toxicity. Of particular interest in this model, the majority of photoreceptors survive until late disease stage, despite the early disappearance of rod outer segments (ROS) (Helmlinger et al., 2004). The survival of photoreceptors distinguishes SCA7 retinopathy from most retinal degenerations in mammals, in which destruction of outer segments is typically followed by photoreceptor cell death (Marc et al., 2003; Marc et al., 2008).

Expression profile analysis of SCA7 R7E retina revealed a global repression of rod photoreceptor specific genes, suggesting that part of dysfunction could be due to a loss of rod differentiation state (Abou-Sleymane et al., 2006). Other deregulated genes belong to pathways

* Corresponding author. Fax: +33 3 88653201.
E-mail address: Yvon.TROTTIER@igbmc.fr (Y. Trottier).
Available online on ScienceDirect (www.sciencedirect.com).

0969-9961/$ – see front matter © 2010 Elsevier Inc. All rights reserved.
doi:10.1016/j.nbd.2010.06.005

such as development, morphogenesis and cell death regulation, suggesting that the toxicity of polyQ-expanded ATXN7 causes a large spectrum of neuronal defects.

Here, we explore the onset, the nature and the extent of rod degeneration in the SCA7 R7E mouse retina by combining electron and light microscopy. We show that the SCA7 retina progressively goes through a complex remodeling process starting early after exposure to polyQ toxic effects. First, in agreement with transcriptomic data we observed that most SCA7 photoreceptors relapse to a morphologically round cell shape with retraction of peripheral components. Second, we show that a subset of rod cells migrate into other retinal layers where they die by a non-apoptotic mechanism reminiscent of dark neuronal death. Resident (non-migrating) rods die by apoptosis. Finally, most remarkably, we detected that some photoreceptors undergo cell division and might temporally replenish the photoreceptor cell population. Therefore, polyQ toxicity can induce a wide range of neuronal responses *in vivo*.

Materials and methods

Animals

SCA7 R7E+/− transgenic mice and their WT littermates were maintained on the inbred C57BL/6 background (Yvert et al., 2000). Genotyping was performed by PCR according to the protocols previously described (Helmlinger et al., 2004). Experiments were approved by the ethical committee C.R.E.M.E.A.S (Comite Regional d'Ethique en Matiere d'Experimentation Animale de Strasbourg).

Histological and electron microscopic analysis

Eyes were fixed by immersion in 2.5% glutaraldehyde and 2.5% formaldehyde in cacodylate buffer (0.1 M, pH 7.4). To facilitate pre-fixation, two small incisions on eye limbs were performed. After 20 min, the lens and cornea were removed and the eyecups were fixed overnight in the same fixative and washed in cacodylate buffer for further 30 min. The eyes were post-fixed in 2% osmium tetroxide in 0.1 M cacodylate buffer for 1 h at 4° C and dehydrated through graded alcohol (50, 70, 90, 100%) and propylene oxide for 30 min each. Samples were oriented and embedded in Epon 812. Semi-thin (2 μm) sagittal sections were cut with an ultramicrotome (Leica Ultracut UCT) and stained with toluidine blue, and histologically analysed by light microscopy. Ultra-thin (70 nm) sections were cut and contrasted with uranyl acetate and lead citrate and examined at 70kv with a Morgagni 268D electron microscope. Images were captured digitally by Mega View III camera (Soft Imaging System) and contrast was adjusted for display purposes.

Immunohistochemistry

Frozen sections from fixed and unfixed retinas were prepared as follow. Eyes were mounted in Tissue Tek O.C.T. (Siemens Medical, Puteaux, France) and frozen with liquid nitrogen immediately after enucleation, or after fixation with 4% formaldehyde in 0.1 M PBS for 2 h. Then, 7–10 μm frozen sections were cut on a Leica CM3050S freezing microtome (Leica, Rueil Malmaison, France). Unfixed sections were used only for anti-centrin 3 immunohistochemistry. Sections were incubated with primary antibodies in 1% BSA in PBS using the following dilutions: 1:250 mouse monoclonal anti-rhodopsin antibody (MAB 5356, Millipore Upstate Chemicon), 1:500 mouse monoclonal anti-phosphohistone 3 antibody (H3-2C5, IGBMC), 1:500 rabbit anti-centrin 3 polyclonal antibody (Trojan et al., 2008), 1:100 rabbit anti-ataxin7 polyclonal antibody (1262) (Yvert et al., 2000), anti-dystrophin antibody (Abcam Ltd). Controls for rabbit polyclonal antisera were non-immune sera used at the corresponding dilution. When monoclonal antibodies were used, control sections were incubated in 1% BSA in PBS. We used goat anti-mouse secondary antibody and goat anti-rabbit secondary antibody (dilution 1: 500) conjugated with Oregon Green or Cy-3 (Jackson ImmunoResearch, West Grove, PA). Nuclei were counterstained with 0.5 μg/ml DAPI (4,6-diaminido-2-phenylindole). Images were acquired with epifluorescent (Leica DM 4000) or confocal (Leica SP2 MP) microscopes. Image brightness and contrast were adjusted for display purposes when necessary.

To estimate the proportion of surviving photoreceptors in PN 42wk SCA7 and WT retina, retinal sections were stained with Hoechst and confocal images were acquired at the level of optic nerve. The number of photoreceptor nuclei per image was counted using segmentation and Timt software.

BrdU injection and immunostaining protocol

Three consecutive intraperitoneal bromodeoxyuridine (BrdU) injections were done every 2 days in 3-week-old SCA7 R7E and WT animals with the standard dose of 50 mg/kg. Enucleated eyes were fixed for 15 min in 4% formaldehyde in PBS, and sectioned as described above. For anti-BrdU immunostaining retinal sections were post-fixed for 5 min in 4% formaldehyde in PBS and incubated in 2 N HCl for 45 min at 37° C. Sections were washed twice in distilled water for 20 min, rinsed in PBS for 20 min, then double immunostained using the mouse monoclonal anti-BrdU antibody (Sigma-Aldrich, dilution 1:500) and the rabbit polyclonal anti-ataxin7 antibody. Secondary antibodies were the same as described in previous section.

TUNEL staining

Frozen sections from unfixed retinas were fixed with 4% formaldehyde in PBS for 1 h at room temperature. After washing

Fig. 1. Progressive deconstruction of SCA7 rod photoreceptors. (A–C) Early and progressive retraction of RIS cytoplasm in ONL. Electron micrograph from PN 6wk WT retina (A) shows that RIS and ONL form distinct layers delimited by an outer limiting membrane (OLM, black arrows), separating cytoplasm of the photoreceptor from the cell body mainly containing the nucleus. In age-matched SCA7 retina (B), RIS cytoplasms are abnormally located in the ONL, even though the OLM appears intact. Occasionally ROS are also observed within SCA7 ONL (C, an inset of B). (D–F) SCA7 rods have a simple cell shape at late disease stages. Electron micrograph from PN 9wk (E) show that some SCA7 rod photoreceptor nuclei are surrounded with a large cytoplasmic compartment containing mitochondria, endoplasmic reticulum and Golgi apparatus, which normally locate in RIS. At PN 39wk (F), most SCA7 rod photoreceptors have entirely retracted the cytoplasmic content from RIS to a perinuclar location and acquire a spherical shape. In the cytoplasm of some rods, a connecting cilium showing 9 + 0 microtubule pairs is observed (inset in F) in transversal section. In comparison to WT retina (D), SCA7 photoreceptor nuclei show important chromatin decondensation (E and F). (G–J) Relocalization of rhodopsin to SCA7 rod cell bodies. Immunofluorescence of PN 20wk WT retina (G) shows that the rhodopsin (green) localizes in ROS. (H) image merged with DAPI stained nuclei (blue). In age-matched SCA7 retina (I), rhodopsin is relocalized in the ONL, where it labels the process (arrow) and entire cell body (arrowhead) of some rods. (J) image merged with DAPI stained nuclei (blue). (K–N) Relocalization of cilia to SCA7 rod cell bodies. Fluorescence images from centrin-3 immunostaining show the presence of photoreceptor ciliary apparati (green) in the junction between the ROS and RIS layers in the WT retina (K) and their relocalization into the ONL of SCA7 retina (L) at PN 40wk. Higher magnifications show that the cilia (arrow) in the SCA7 ONL (M, an inset of L) are definitively larger in size than centriole pairs detected in the control INL (N, arrowhead). Images are merged with Hoescht stained nuclei (red) and represent projections of confocal slices. (O and P) Reduced density and delocalization of SCA7 synapses. Fluorescence images of dystrophin immunostaining show the photoreceptor synapses (green) in WT OPL (O) and their reduced density in SCA7 OPL at 42 weeks of age (P). Some SCA7 rod synapses (arrowhead) are mislocated in the ONL. Images are merged with Hoechst stained nuclei (red). (Q) Schematic illustrating the deconstruction of differentiated rods into a morphologically simpler cell shape. Morphological changes involve disappearance of ROS, retraction of the entire cytoplasmic content of RIS to perinuclear location and reorganization of the nuclear architecture. Some deconstructed rods seem to loose their synapses, while others conserve normal synapses and a vestige of connecting cilium. Abbreviations: ONL and INL, outer and inner nuclear layers; ROS and RIS, rod outer and inner segments; OPL, outer plexiform layer; RPE, retinal pigmented epithelium. Scale bar: 4 μm (A and B); 2 μm (C–F); 20 μm (G–L, O, and P); 5 μm (M and N).

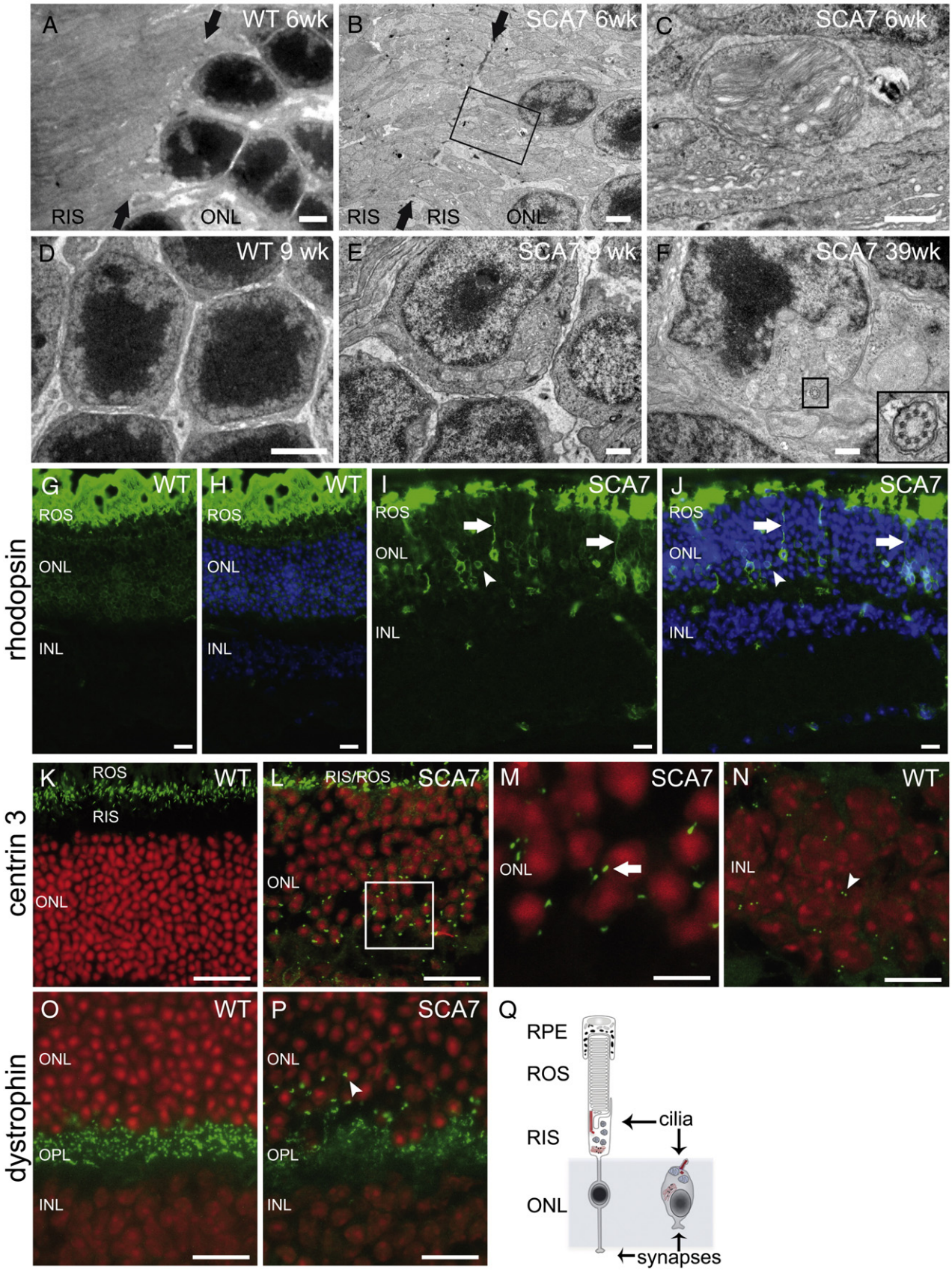
A
WT 6wk
RIS
ONL
B
SCA7 6wk
RIS
RIS
ONL
C
SCA7 6wk
D
WT 9 wk
E
SCA7 9 wk
F
SCA7 39wk
rhodopsin
G
WT
ROS
ONL
INL
H
WT
ROS
ONL
INL
I
SCA7
ROS
ONL
INL
J
SCA7
ROS
ONL
INL
centrin 3
K
ROS
WT
RIS
ONL
L
RIS/ROS
SCA7
ONL
M
SCA7
ONL
N
WT
INL
dystrophin
O
WT
ONL
OPL
INL
P
SCA7
ONL
OPL
INL
Q
RPE
ROS
RIS
ONL
cilia
synapses

sections were incubated with 0.3% Triton X-100/PBS for 20 min, then processed for TUNEL staining according manufacturer protocol (Roche Applied Science).

Quantifications

Quantification was generally performed from 4 to 10 retinal sections/mouse using 3–6 mice/genotype-age, unless indicated. Statistical analyses were done using one-way or two-way ANOVA followed by Bonferroni posthoc test.

Retinal fractionation and Western blot analysis

Fractionation of SDS soluble and SDS insoluble proteins and formic acid treatment were as described before (Lunkes et al., 2002). Briefly, whole retinal proteins were solubilized in a SDS buffer (2% SDS, 5% ß-mercaptoethanol, 15% glycerol), denatured by boiling for 10 min and sonicated as described (Lunkes et al., 2002). SDS soluble and SDS insoluble protein were separated by centrifugation at 15 000 × *g* 15 min. The resulting pellet was washed three time with SDS buffer. Pellet was solubilized using 100% formic acid and incubated at 37° C for 30 min. Formic acid was dried in speed-vac and the resulting dried material was resuspended in Laemmli loading buffer prior to Western blot analysis. Anti-rhodopsin antibody (1D4 from Millipore) was diluted at 1:10 000; 1C2 antibody at 1:200; anti-ATXN7 polysera (1262) at 1:200; anti-ATXN7 monoclonal (1C1) at 1:1000; anti-ß-tubulin at 1:10 000. For stripping, membranes were incubated in denaturing buffer (50 mM Tris–HCl pH 6.8, 2% SDS, 5% ß-mercaptoethanol) at 50° C for 30 min.

Results

SCA7 rods undergo morphological transformation into round cell shape

Initial studies reported that SCA7 R7E retinopathy starts at 4 weeks post-natal (PN 4wk) with a reduction of ERG and thinning of ROS (Helmlinger et al., 2004; Yvert et al., 2000). It slowly progresses up to flat ERG response and almost complete absence of ROS layer at late disease stage (>1 year of age), without major reduction of the outer nuclear layer (ONL) thickness (Helmlinger et al., 2004; Yvert et al., 2000); photoreceptor survival was roughly estimated at 70% at 13 months of age (Yvert et al., 2000). Consistent with this, a careful quantification indicated that 80% of the photoreceptors survive after 11 months of disease duration (Supplementary Fig. 1), and therefore several months after disappearance of segments.

Transcriptional repression affects a large cohort of genes involved in phototransduction and segment morphogenesis, suggesting that the renewal of functional ROS is compromised and rod photoreceptors relapse to immature rod cell phenotype (Abou-Sleymane et al., 2006). We wanted to examine the modus operandi underlying photoreceptors remodeling in SCA7 mouse retina. At early disease stages (PN 4–6wk), electron microscopy (EM) analysis revealed the abnormal presence of rod inner segments (RIS) in the ONL, right beyond the outer limiting membrane (OLM) (Fig. 1B). From PN 6wk, the presence of RIS augmented in the ONL of the peripheral retina where the disease progressed more rapidly (data not shown). In some cases, we even observed the abnormal presence of ROS in the ONL (Fig. 1B and C). The retraction of RIS and ROS into the SCA7 ONL was not due to disruption of the OLM, since its integrity appeared normal on electron micrographs (Fig. 1A and B, arrows).

RIS retraction might represent the initial phase of rod deconstruction, causing the re-distribution of the cytoplasmic content around the nucleus. To highlight this process, we performed immunofluorescence analysis using an antibody against rhodopsin, a membrane protein (Fig. 1G–J). In WT situation, rhodopsin was massively located in ROS (Fig. 1G and H), and displayed a very faint labeling in the ONL. In 20-week-old SCA7 retina, rhodopsin labeling was reduced in the ROS layer due to the down-regulation of rhodopsin gene and the important loss of ROS at this time point (Helmlinger et al., 2004). More importantly, rhodopsin labeling also outlined the plasma membrane of retracting processes (Fig. 1I and J, arrows) and in some cases, of entire cell bodies of rods in the SCA7 ONL (Fig. 1I and J, arrowhead), suggesting a structural reorganization of rod plasma membrane.

EM analysis at late disease stage (39 weeks of age) showed that SCA7 rod photoreceptors lost polarity, entirely retracted their cytoplasmic content to a perinuclear location and acquired a spherical shape (Fig. 1F). The cytoplasm contained normal endoplasmic reticulum, Golgi apparatus and mitochondria. Almost all rod nuclei at this age showed important chromatin decondensation as reported previously (Helmlinger et al., 2006). Round rod cells with decondensed chromatin were already seen as early as PN 9wk (Fig. 1E), although they were less prominent and heterogeneously distributed in the retina.

Interestingly, we observed on electron micrograph the presence of connecting cilia with the characteristic structure of nine microtubule doublets in the perinuclear cytoplasm of some SCA7 rod cells (Fig. 1F and inset). This suggested that SCA7 rods retract their connecting cilia along with the cytoplasm and maintain them despite the deconstruction phenotype. To confirm the presence of photoreceptor cilia in the ONL, we performed immunofluorescence studies with an antibody against centrin 3. Centrin 3 is a component of ciliary apparatus of photoreceptor cells and localizes in the connecting cilium, the basal body and the adjacent centriole (Giessl et al., 2004; Trojan et al., 2008). Fig. 1K shows that centrin 3 antibody specifically detected ciliary apparati at the junction between RIS and ROS in WT retina. In SCA7 retina, the density of cilia in the residual segment layer was lower than in WT and cilia were located proximally to the ONL. More interestingly, cilia were detected in SCA7 ONL, while WT ONL was strictly devoid of cilia (Fig. 1K–N). We then reasoned that cilia relocalization in the ONL would represent an excellent marker to quantify the progressive rod deconstruction along the SCA7 disease progression. Therefore, we analysed the percentage of SCA7 rods harboring cilia inside the ONL at different disease stages. Cilia were not found in the ONL at PN 3wk, however, their occurrence progressively increased in this layer from PN 6–40wk. At the latest disease stage, 42% of SCA7 rods harbored a cilium inside the ONL (Fig. 2 and Supplementary Fig. 2).

Finally we explored whether SCA7 rods maintain their synaptic contacts with horizontal and bipolar neurons. At EM level, rod synapses in the outer plexiform layer (OPL) of SCA7 retina were structurally normal, but their number appeared slightly lower than in WT OPL (data not shown). This was confirmed by immunofluorescence with an antibody against dystrophin, which labels both cone and rod synapses. At PN 3wk and 9wk, the density of synapses in SCA7 OPL was comparable to WT, but slightly decreased from PN 20wk (Fig. 1O and P, and data not shown). Moreover, at 42 weeks of age some ectopic synapses invaded SCA7 ONL (Fig. 1P), consistent with earlier observations showing that horizontal and rod-bipolar neurons had neurites infiltrating the ONL (Yvert et al., 2000).

Together, these results trace the profound morphological transformation of SCA7 rod photoreceptors into a round cell shape (Fig. 1Q).

SCA7 rods migrate outward the ONL and die at late stages

Despite the atypical cell shape at late disease stages, SCA7 rods in the ONL appear healthy, as the structural integrity of their organelles remains normal. In contrast, we observed that some cells located in the segment layer (ROS and RIS) showed degenerative signs (see below). Yvert et al. (2000) reported the presence of ectopic cells in the SCA7 R7E retina, but their identity and frequency were unknown. Therefore, we studied the origin, frequency, and fate of these ectopic cells in SCA7 retina.

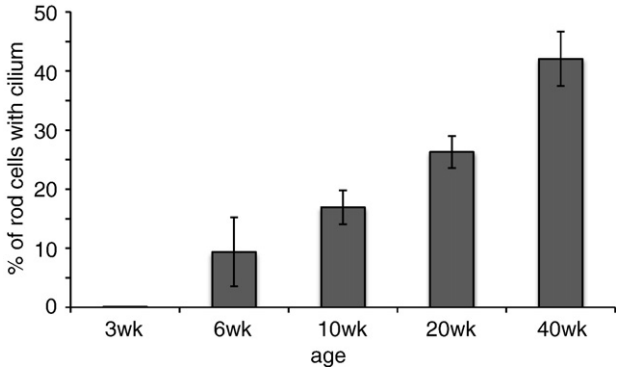

Fig. 2. Quantification of SCA7 rods harboring cilia inside the ONL at different disease stages. Percentage of SCA7 rods harboring cilia, as revealed using centrin-3 antibody, increases with the disease progression (mean ± SD, $n = 3$ mice per age). $p < 0.0001$ by one-way ANOVA analysis.

On histological semi-thin sections, we detected ectopic cells from PN 2–39wk (Fig. 3). They were located in the segment layer, in the OPL and in the inner nuclear layer (INL). At PN 2wk (Fig. 3B and D), ectopic cells represented scattered events along the retinal sections. They were located in regions that showed reduced thickness of segment layer. By PN 4wk (Fig. 3H), they were readily detected in regions where photoreceptor segments showed irregularities. From PN 9wk (Fig. 3I), their number increased considerably, concomitant with the extension of segment irregularities. At late disease stage (39 weeks), numerous ectopic cells were found in the residual segment layers all along retinal sections (Fig. 3J). We quantified the number of ectopic cells in the segment layer at different disease stages. Only these ectopic cells were evaluated, as counting was facilitated by the usual absence of cell nuclei in this layer. While we found no ectopic cell/section in WT retina at any age ($n = 4$ mice), the number of ectopic cells strongly increased in the SCA7 retina from PN 4–42wk: $0{,}2 \pm 0{,}2$ cells/section at PN 3–4wk, 32 ± 4 cells/section at PN 9–10wk and 64 ± 4 cells/section at PN 38–42wk (mean ± SD) (Supplementary Table 1).

In other retinal degenerations, ectopic cells were described to originate from the aberrant migration of glial Müller cells and bipolar cells (Fischer and Reh, 2001; Marc et al., 2008). However, light microscopy revealed that ectopic cells in PN 2wk SCA7 retina had characteristics of rod cells, with highly compact nuclei surrounded by a thin cytoplasmic layer and containing one to three large heterochromatin foci (Fig. 3E and F). Ectopic cells with typical rod nuclei were also observed by electron microscopy (Fig. 4A). In addition, we observed rhodopsin-positive cells in the SCA7 INL (Supplementary Fig. 3), hence supporting the fact that some SCA7 rods aberrantly migrated in the INL. In contrast, rhodopsin-positive cells were never detected in the INL of WT retina (see Fig. 1G and H).

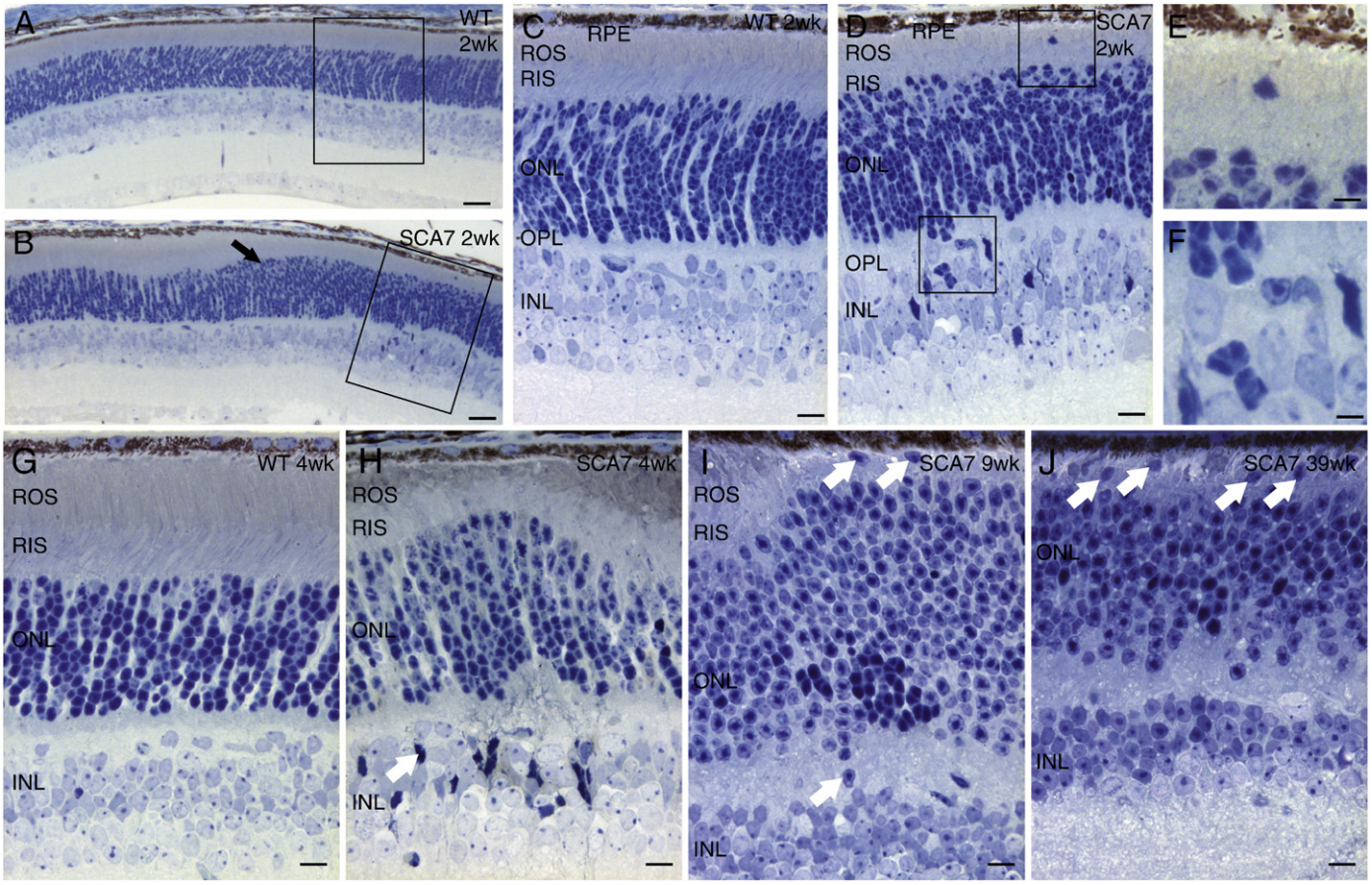

Fig. 3. Presence of ectopic cells in the SCA7 retina from early to late disease stages. (A–F) Histological analysis (semi-thin section) of WT retina at PN 2wk (A) shows a typical regular lamellar organization. (C) is an inset of (A). In SCA7 retina at PN 2wk (B), some regions display thickness irregularities of ONL (arrow) and shortening of ROS, where ectopic cells can be observed in the INL, OPL and RIS/ROS layers. (D) is an inset of B. Ectopic cells in the INL and OPL (E, an inset of D) as well as in RIS/ROS layers (F, an inset of D) present highly compact nuclei containing one to three heterochromatin foci, similar to rod photoreceptor nuclei of ONL. (G–J) Ectopic cells (white arrow) are observed in semi-thin section of SCA7 retina of all disease stages analysed, including PN 4wk (H), 9wk (I) and 39wk (J), but not in the PN 4wk (G) and older WT retina (data not shown). SCA7 ectopic cells are generally found in regions showing irregularity of ONL thickness and organization. Note that images in (G–J) are from non-equivalent regions of retinal sections. Abbreviations: ONL and INL, outer and inner nuclear layers; ROS and RIS, rod outer and inner segments; OPL and IPL, outer and inner plexiform layers; RPE, retinal pigmented epithelium. Scale bar: 50 μm (A and B); 12 μm (C and D); 8 μm (E and F); 17 μm (G–J).

Other observations at later disease stages also indicate that ectopic cells correspond to SCA7 rod cells that migrated out of the ONL. Fig. 4B (arrow) shows an example of a PN 9wk rod cell that seemed to migrate through the OLM, from the ONL toward the segment layers. In addition, a nearby ectopic cell (ec) contained pale nuclear structure (arrowhead), which likely represents aggregates formed by mutant ATXN7. Finally, Fig. 4C and D show that ectopic cells in the segment layer contained a connecting cilium, a typical photoreceptor organelle. We then performed immunofluorescence analysis using ATXN7 and centrin-3 antibodies at different disease stages to estimate the proportion of ectopic cells in the segment layer harboring NI and cilia. We found that all ectopic cells in the segment layer of PN 9–10wk and 28–42wk retina contained ATXN7 NI and cilia (Supplementary Table 1).

From PN 9wk, ectopic rod photoreceptors showed signs of morphological transformation similar to rods in ONL. They had large perinuclear cytoplasm with numerous swollen mitochondria and the chromatin appeared decondensed (Fig. 4B, C, and E). In addition, many ectopic photoreceptors in the segment layer were dying as they

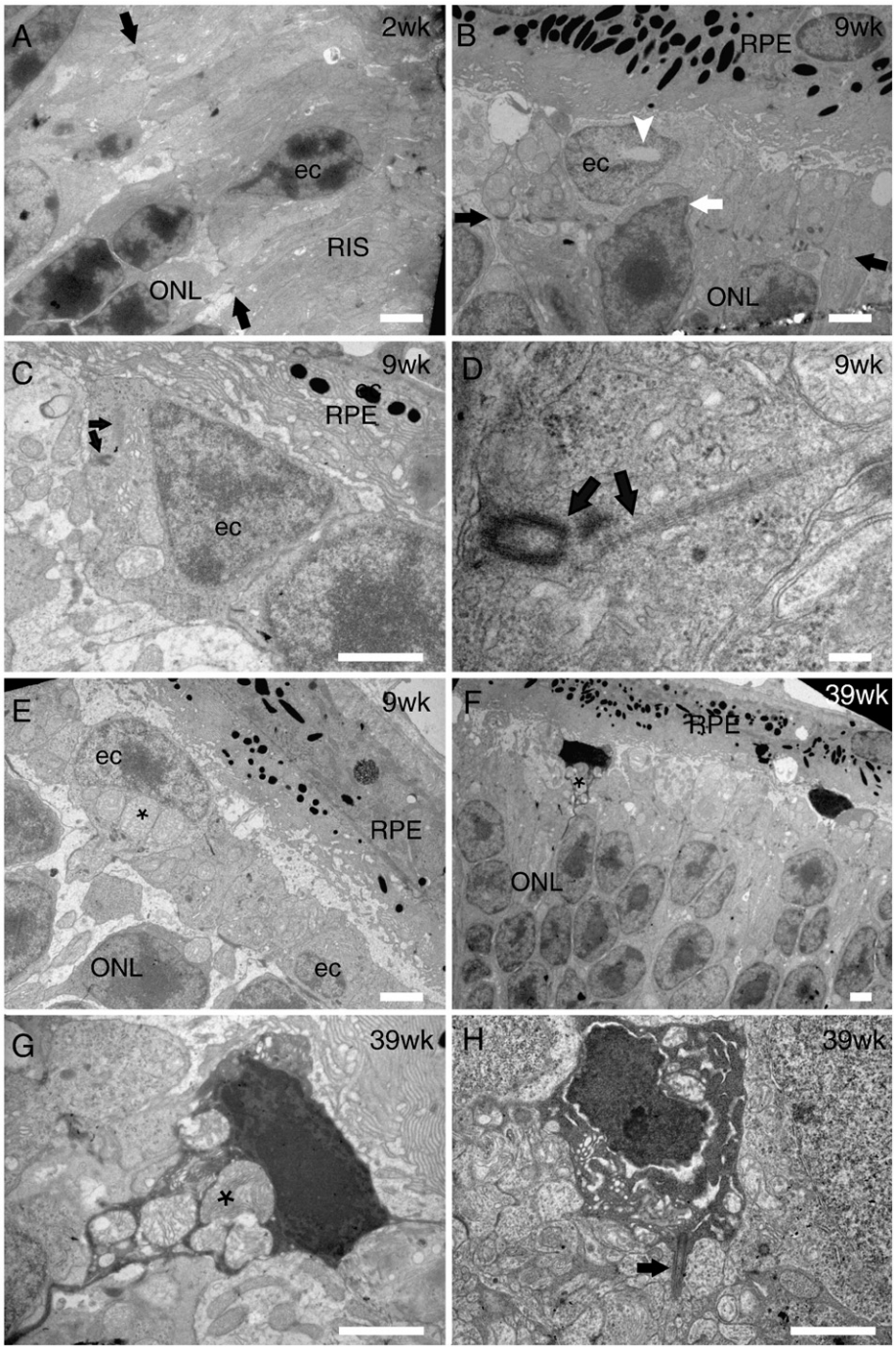

Fig. 4. Ectopic cells are rods that degenerated at late disease stages. (A–D) Electron micrograph from PN 2wk SCA7 retina (A) shows an ectopic cell nucleus (ec) located in the segment layer, with the typical compacted chromatin of rod cells (black arrows indicate the OLM). At PN 9wk, ectopic cells contain either nuclear pale structure that are ATXN7 aggregates (B, white arrowhead) or a connecting cilium (C, black arrows, and D, a higher magnification), indicating they are rods. An example of rod cell migrating from ONL to the segment layer is shown in (B, white arrow). Ectopic rods shown in (B), (C) and (E) display chromatin decondensation and perinuclear cytoplasm similar to some SCA7 rods in the ONL at this disease stage (see Fig. 1E and F). (E–H) Some ectopic cells present swollen mitochondria (asterisk) at PN 9wk (E). At PN 39wk, ectopic cells are dying and show degenerating mitochondria (asterisk) and darkly stained nuclei (F and G, a higher magnification). Similarly, degenerating darkly stained cells, containing a connecting cilium (arrow) are observed in INL as well (H). Abbreviations: ONL, outer nuclear layers; ec, ectopic cell; RIS, rod inner segment; RPE, retinal pigmented epithelium. Scale bar: 5 μm (A–C, E, and F–H); 0.5 μm (D).

had degenerated mitochondria and darkly stained nuclei with clumping of chromatin (Fig. 4F and G). We estimated that 50–70% of ectopic cells in the segment layer of PN 9–42wk retina displayed degenerative signs (Supplementary Table 1). These ectopic dying cells were neither stained by TUNEL and anti-activated caspase 3 antibody, nor by autophagy markers on immunohistochemistry (data not shown). Similarly in the INL of SCA7 retina, we observed darkly stained cells with degenerative signs. These cells contained connecting cilia (Fig. 4H, arrow), suggesting their photoreceptor origin.

Together, these results show that an increasing proportion of SCA7 rod photoreceptors migrate out of the ONL towards the inner retina and segment layer. Ectopic rod photoreceptors die by a non-apoptotic mechanism reminiscent of dark neuronal cell death. None of these degenerative anomalies was observed in the age-matched WT retina.

A subset of SCA7 rods in the ONL degenerates at early stages

We found that some morphological anomalies of SCA7 R7E retina occurred already at PN 2wk (Fig. 3B). Not only the segment layers were reduced, but also the thickness of the ONL was irregular in some areas and the linear organization of photoreceptor nuclei along the width of the ONL was perturbed when compared to WT (Fig. 3A). These early defects are nevertheless consistent with the fact that mutant ATXN7, which is under the rhodopsin promoter, is likely expressed from PN 1 day, and rods should be exposed to polyglutamine toxicity very early in the development, long before their terminal differentiation (Treisman et al., 1988).

To get insight into early stages of SCA7 retinopathy, we performed a careful examination of the retinal structure by EM. From PN 2wk, we confirmed that the ROS layer in SCA7 was occasionally shorter and less densely packed than in WT mice (Fig. 5A and B). Two weeks later (PN 4wk), scattered ROS were disorganized, lost their parallel orientation (Fig. 5D) and contained degenerating vesicular lamellae (Fig. 5F, arrowhead), contrasting with WT retina (Fig. 5C). In addition, some degenerating RIS presented darker cytoplasm with abnormal mitochondria (Fig. 5D, arrowheads). Degenerating RIS were also frequent at PN 6wk, but their occurrence were also decreased at later disease stages (Fig. 5E and Supplementary Table 1).

Fig. 5G shows dark degenerating RIS with dilatation and vesiculation of endoplasmic reticulum that was clearly linked to its photoreceptor cell nucleus inside the ONL, indicating that not only the segments but also the entire rod cell were degenerating. Other photoreceptors in the ONL were even darker and likely more advanced in the process of degeneration (Fig. 5H). They had atrophic nuclei with atypical scalloped shape and displayed clumping of chromatin. They showed no fragmentation or “blebbing” features associated to apoptotic-like mechanism. Adjacent neurons were of normal appearance. Dark photoreceptors were readily observed in the ONL of 4- and 9-week-old SCA7 mice. They were less frequent later on but could nevertheless be observed until late time points (Supplementary Table 1). Dark photoreceptors were never observed in WT littermate. These dying rods looked similar to the darkly degenerating ectopic rods observed at later time points (Fig. 4F–H).

Electron microscopy inspection of SCA7 ONL also revealed several photoreceptors with round-shaped nuclei and highly condensed chromatin, reminiscent of apoptotic nuclei (Fig. 6A). Using TUNEL staining, we compared the level of apoptosis in WT and SCA7 ONL (Fig. 6B and C). Consistent with previous study (Vecino et al., 2004), apoptotic nuclei were sporadically detected in WT PN 2–3wk, and became very rare later on (Fig. 6D). The level of apoptosis was significantly higher in SCA7 than in WT from PN 2–6wk. SCA7 apoptosis significantly increased from PN 1.5wk to 2–3wk, and then decreased over time, contrasting with the disease aggravation.

Together, these results indicate that a subset of photoreceptors degenerate and die in the ONL at very early disease stages. Two different mechanisms are involved: a non-apoptotic darkly stained neuronal death and apoptosis.

SCA7 rods in the ONL undergo cell division at early disease stages

Our data indicate that there is a significant rate of photoreceptor cell death in SCA7 R7E retina. Cell death affects rods in the ONL at early disease stages and migrating rods at later disease stages. Therefore, we wondered why the number of photoreceptor cells is only modestly reduced. A clue came from the observation of centriole-like structures adjacent to nuclei of rod photoreceptors showing unusually large perinuclear cytoplasms (Supplementary Fig. 4). Occasional centriole pairs in the ONL were confirmed by immunofluorescence using anti-centrin-3 antibody (Supplementary Fig. 4). The presence of centriole pairs could license photoreceptors for mitotic division, raising the possibility that SCA7 rods might undergo cell proliferation.

In order to verify rod cell division, PN 4wk SCA7 and WT animals were injected with BrdU. Basal cells of cornea epithelium, which continuously proliferate in adult eyes stained positively with BrdU and served as internal positive control (data not shown). BrdU-positive cells were observed in the ONL of SCA7 R7E retina, but not in WT (Fig. 7A–D). We counted 12 ± 3 (mean $\pm$ SD, $n = 3$ mice) BrdU-positive cells/retinal section in SCA7 retina, while no BrdU-positive cell ($n = 3$ mice) was observed in the ONL of WT (t test: $p = 0{,}0013$). Co-labeling with ATXN7 revealed that BrdU-positive cells expressed mutant ATXN7 (Fig. 7E–J). At this early time point, rod photoreceptors of the outermost part of the ONL contained ATXN7 nuclear inclusions (NI), while those in the innermost part displayed a homogenous labeling, because ATXN7 is not yet aggregated. Photoreceptors containing NI or soluble ATXN7 had incorporated BrdU (data not shown).

Since BrdU can be incorporated during S-phase DNA synthesis or DNA repair, it did not warrant that positive cells were dividing. To confirm cell division of rod photoreceptors, we used an antibody against phosphorylated histone 3 (PH3), a proliferation marker expressed from late G2 to anaphase (Hendzel et al., 1997). Immunostaining of WT retina with anti-PH3 antibody only labeled proliferative basal cells of cornea epithelium (data not shown) and blood vessels in the inner retina (Fig. 8A–C, arrowheads). In contrast, PH3-positive cells were readily detected within the ONL of PN 3wk SCA7 retina (Fig. 8D–F, arrows). Co-labeling revealed that PH3-positive cells contained ATXN7 in aggregated or soluble form (Fig. 8G–I and data not shown). PH3-positive cells were present in the central and peripheral retina. Quantification showed that the number of PH3-positive cells was high in PN 3wk SCA7 retina but it significantly decreased at 6 and 9 weeks of age (Fig. 8L). PH3 labeling was absent in the ONL of age-matched WT retina.

Finally, we observed mitotic figures in the ONL of SCA7 retina at the EM level. We found examples of daughter cells in telophase going through cytokinesis (Fig. 8J and K), indicating that SCA7 rod photoreceptors were not blocked at any stage of cell cycle and successfully went through a complete mitotic division. Together, these results indicate that a subset of SCA7 rod photoreceptors undergo cell division at early disease stages, suggesting that new rod cells compensate cell death occurring at these time points.

Different patterns of mutant ATXN7 species are associated with early and late disease stages

Apoptosis and cell division peaked during early disease stages (PN 2–3wk) and decreased later on, whereas cell migration, dark neurodegeneration of ectopic cells and rod deconstruction aggravated with mouse age. The various cellular responses may be triggered by the presence of different potentially toxic species of polyQ-expanded ATXN7, such as full-length, proteolytic fragments, soluble and insoluble aggregates. Therefore, we analysed the temporal expression pattern of ATXN7 species in the retina using biochemical fractionation

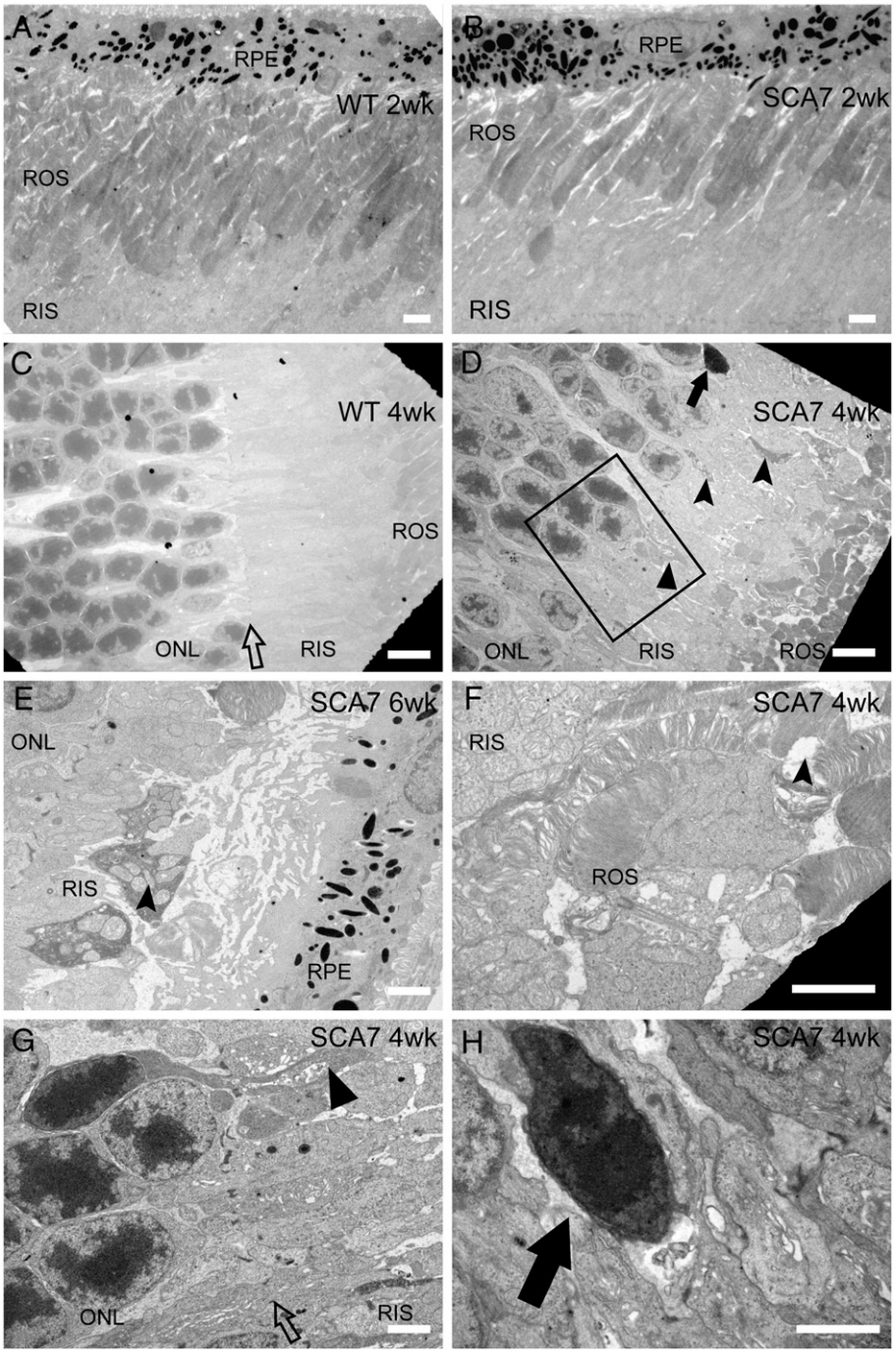

Fig. 5. Dark degeneration of SCA7 rods at early stages. (A and B) Electron micrograph from PN 2wk SCA7 retina (B) shows shorter and less densely packed ROS than age-matched WT retina (A). (C–H) While PN 4wk WT retina presents a regular organization of ONL, RIS and ROS (C), age-matched SCA7 retina shows several signs of photoreceptor degeneration (D and F–H). Some ROS lose their parallel organization (D) and present degenerating vesicular lamellae (F, arrowhead). Degenerating RIS with darker cytoplasm and abnormal mitochondria are occasionally observed (D, arrowhead) at this disease stage and become more frequent at PN 6wk (E, arrowhead) in regions where ROS have disappeared. Electron micrograph in G (which is an inset of D) shows an example of degenerating rod photoreceptor that displays darkly stained nucleus and RIS (black arrowhead); RIS cytoplasm contains dilated and vesiculated endoplasmic reticulum. Other rod photoreceptor nuclei are even darker (an example in H, which corresponds to the black arrow in D), display atypical scalloped shape and chromatin clumping, suggesting they are more advance in the degenerative process. Open arrows in C and G show the OLM. Abbreviations: ONL, outer nuclear layer; ROS and RIS, rod outer and inner segments; RPE, retinal pigmented epithelium; OLM, outer limiting membrane. Scale bar: 5 μm (A, B, and E–H); 12.5 μm (C and D).

of SDS soluble and insoluble proteins (Lunkes et al., 2002). Proteins were analysed on Western blot using anti-ATXN7 antibody and 1C2 anti-polyQ antibody that specifically reveals the polyQ-expanded ATXN7 transprotein. In the SDS soluble fraction, full-length mutant ATXN7, revealed by 1C2, showed an expression pattern very similar to rhodopsin (Fig. 9A and B). Both proteins were highly expressed at PN 2–3wk, and their expression level decreased with age due to the progressive repression of rhodopsin promoter, correlating with loss of rod differentiation phenotype. In contrast to rhodopsin, full-length mutant ATXN7 was undetectable at 20–40 weeks of age, even after prolonged exposure.

At PN 2–3wk 1C2 also revealed several soluble proteolytic fragments of mutant ATXN7 (a, b, c and d in Fig. 9B) as well as a high molecular weight smear running above 250 kDa. These proteolytic fragments and high molecular weight smear were not detected from 11 to 40 weeks. However, probing the same Western blot with

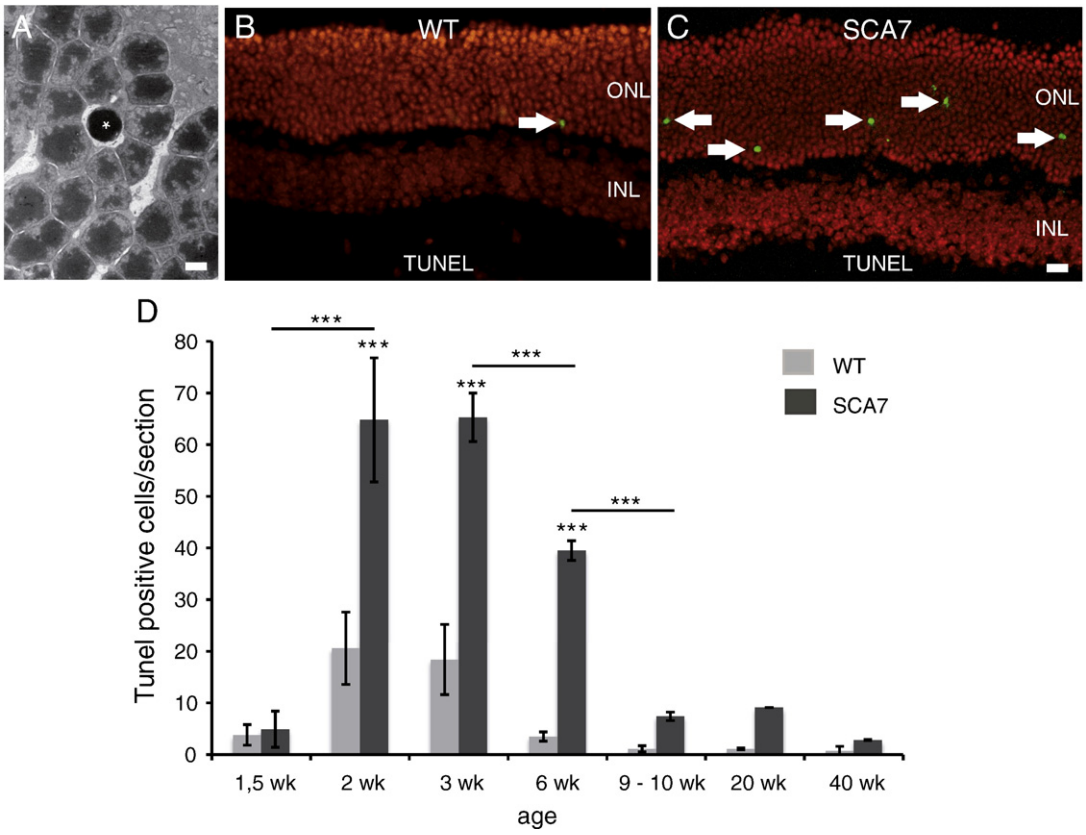

Fig. 6. Apoptotic cell death of SCA7 rods at early stages. (A) Electron micrograph of an apoptotic photoreceptor nucleus (asterisk) with round shape and highly condensed chromatin in the ONL. Representative fluorescence of TUNEL-positive nuclei (green, white arrows) in the ONL of PN 3wk WT (B) and SCA7 (C) retina (images merged with DAPI stained nuclei (red)). (D) Quantification of TUNEL-positive nuclei in the ONL of WT and SCA7 retina at different ages (mean ± S.D., $n = 4$–6 mice for PN 1.5–9wk, and $n = 2$ for PN 20wk and 40wk). There is significantly more TUNEL-positive nuclei in SCA7 ONL than in WT ONL at PN 2–6wk. There is significantly more TUNEL-positive nuclei in SCA7 ONL at PN 2–6wk than at PN 1.5wk or PN 9–10wk. ***, $p<0.001$ by ANOVA with Bonferroni posthoc analysis. Abbreviations: ONL and INL, outer and inner nuclear layers. Scale bar : 4.5 μm (A); 25 μm (C).

an anti-ATXN7 antibody revealed the accumulation of insoluble material in the wells of SDS-PAGE only at 11 to 40 weeks of age (Fig. 9C). This material may represent insoluble fibrillar forms of ATXN7 that were not entirely pelleted by centrifugation. In agreement with this, 1C2 antibody, which does not recognize fibrillar polyQ aggregates, did not reveal this material in the wells (data not shown).

The pelleted SDS insoluble fraction was solubilized using formic acid treatment (Lunkes et al., 2002) prior to Western blot analysis with anti-ATXN7 antibody. Fig. 9D shows several bands at PN 2–3wk, which have molecular weights corresponding to full-length ATXN7 and its proteolytic fragments a, b, c and d already observed in the SDS soluble fraction at the same ages (Fig. 9B). Moreover, an additional band (band e in Fig. 9D) corresponding to a shorter ATXN7 fragment was detected at PN 2–3wk in the formic acid soluble fraction, but was not seen in the SDS soluble fraction (data not shown). Only this band was observed in the formic acid soluble fraction at 11–40 weeks of age, and its relative intensity strongly increased with age.

Therefore, the pattern of ATXN7 species in the retina largely differs from early to late disease stages. PN 2–3wk retina have full-length and several proteolytic fragments of mutant ATXN7 in either soluble or insoluble forms. In contrast, PN 20–40wk retina contain only one insoluble ATXN7 fragment, while species present at earlier stages are undetectable. In addition, a smear of high molecular weight soluble ATXN7 species is detected only in PN 2–3wk retina, while presumably fibrillar ATXN7 aggregates are present only in PN 20–40wk retina. ATXN7 species in PN 11wk retina might be representative of a transition period between early and late disease stages, as soluble full-length mutant ATXN7 and presumably fibrillar ATXN7 aggregates are present at the same time while only one fragment in its insoluble form is detected.

Discussion

Complex retinal remodeling in SCA7 mouse

In most retinal degenerations triggered by gene mutations or environmental factors, photoreceptors are the primary target, although the rate of photoreceptor loss varies considerably (Jones et al., 2003). For instance, in commonly used genetic models complete loss of photoreceptors can happen at 20 days in *rd1* mice (Pittler and Baehr, 1991) or at up to 12 months in *Rds* (Travis et al., 1992). However, the succession of degenerative events is relatively similar. It generally initiates by a destruction of outer segment that is typically followed by photoreceptor cell death and then proceeds through a profound remodeling of neural retina remnants (Marc et al., 2003). The SCA7 R7E retina shows an atypical scheme of degeneration, since photoreceptor loss is limited despite the almost complete absence of segments, recognizing this retinopathy as one of the slowest retinal degeneration described in mouse. Here, we show that another peculiarity of SCA7 retinopathy is the wide range of degenerative and remodeling features, which include apoptotic and non-apoptotic cell death, cell division, migration and morphological transformation leading to loss of differentiation phenotype.

Most SCA7 photoreceptors relapse to a morphologically simpler cell shape (Fig. 1Q), which correlates with prolonged survival against polyQ toxicity but at the expense of rod function. Such protective deconstruction is atypical in mammalian retinal degenerations. It has been only reported for rod in the feline model of retinal detachment (Fisher et al., 2005) and in retinitis pigmentosa models treated with CNTF (Beltran et al., 2007; Bok et al., 2002; Liang et al., 2001; Rhee

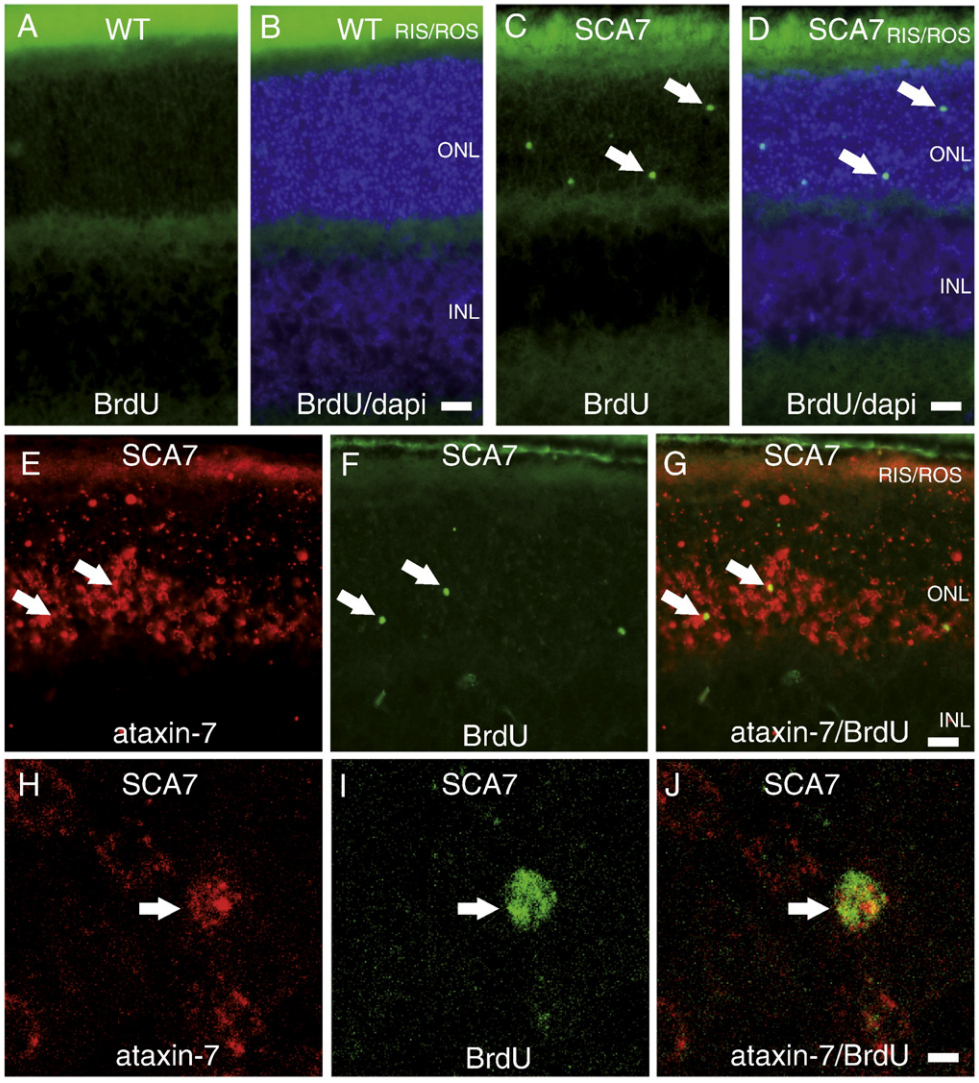

Fig. 7. Bromodeoxyuridine incorporation in SCA7 rods at early stages. (A–D) SCA7 rods incorporate the DNA synthesis marker bromodeoxyuridine (BrdU). BrdU immunostaining reveals the presence of positive cells (arrows) in the SCA7 ONL at PN 4wk (C and D), but not in the age-matched WT ONL (A and B). (E–G) BrdU positive cells (F) in SCA7 ONL are co-labeled with ATXN7 immunostaining (E). G is merged images. (H–J) An example of colocalization of ATXN7 NI (H) and BrdU (I) is shown magnified. J is merged images. Images are projection of confocal slices. Abbreviations: ONL and INL, outer and inner nuclear layer; ROS and RIS, rod outer and inner segments. Scale bar: 30 μm (A–G); 2.5 μm (H–J).

et al., 2007), and for cone in *rd1* mouse retina (Lin et al., 2009). Cilia relocalization into the ONL, which was not observed during the rapid retinal degeneration of RD10 mouse (unpublished results), might represent an excellent marker to detect photoreceptor deconstruction events in retinopathies that display limited cell loss akin SCA7. Identification of specific mechanisms underlying photoreceptor deconstruction is thus warranted to understand the physiopathology of these diseases. The maintenance of vestige of differentiation, such as the cilium and synapse in some SCA7 rods, raises an interesting question about the neuronal regenerative potential.

We show that substantial photoreceptor cell death occurs in SCA7 retina, via at least two mechanisms: apoptosis and darkly stained neuronal death. The former is commonly triggered during retinal degeneration (Lohr et al., 2006). However, the latter is a yet poorly described non-apoptotic mechanism (Kovesdi et al., 2007). Darkly stained neuronal death was reported in other polyQ disorders (Custer et al., 2006; Gray et al., 2008; Turmaine et al., 2000), but yet the underlying mechanism is unclear. The spectrum of progressive cell darkening we observed suggests that death occurs over a period of days rather than hours. The progressive cell darkening excludes the possibility that they represent histological artefacts (Jortner, 2006). Prior to darkly stained neuronal death, rods migrate outside the ONL towards inner retina and subretinal space. Migration requires that rods loose their tight contacts with neighbors. Modification in cell adhesiveness might be a consequence of rod cell reshaping during deconstruction or cell division. Cell death occurring at early disease

Fig. 8. SCA7 rods labeling by phospho-histone H3 mitotic marker at early stages. (A–C) In PN 3wk WT retina, phospho-histone H3 (PH3) immunostaining reveals blood vessels in the inner retina (arrowheads), but no labeling in the ONL. (D–F) In contrast, PH3-positive cells (arrows) are detected in age-matched SCA7 ONL that co-labeled with ATXN7 immunostaining. (G–I) An example of colocalization of ATXN7 NI (G, merged with Hoechst blue staining) and PH3 labeling (H) is shown magnified. C, F and I are merged images. G-I are projection of confocal slices. (J and K) Electron micrographs of a mitotic figure in PN 3wk SCA7 retina. (J) Daughter photoreceptor cells in late telophase going through cytokinesis are migrating through the outer limiting membrane (black arrows), toward the segment layer. (K) The mitotic furrow (arrowhead) is shown magnified. (L) Quantification of PH3-positive cells in the ONL of WT and SCA7 retina at different ages (mean ± S.D.). There is significantly more PH3-positive cells in SCA7 ONL than in WT ONL at PN 3wk, 6wk and 9wk. PH3-positive cells significantly decreased in SCA7 ONL at PN 6wk and 9wk. ***, $p<0.001$; *, $p<0.05$ by ANOVA with Bonferroni posthoc analysis. Abbreviations: ONL and INL, outer and inner nuclear layer; ROS and RIS, rod outer and inner segments. Scale bar : 30 μm (A–F); 2.5 μm (G–I); 3 μm (M); 0.5 μm (N).

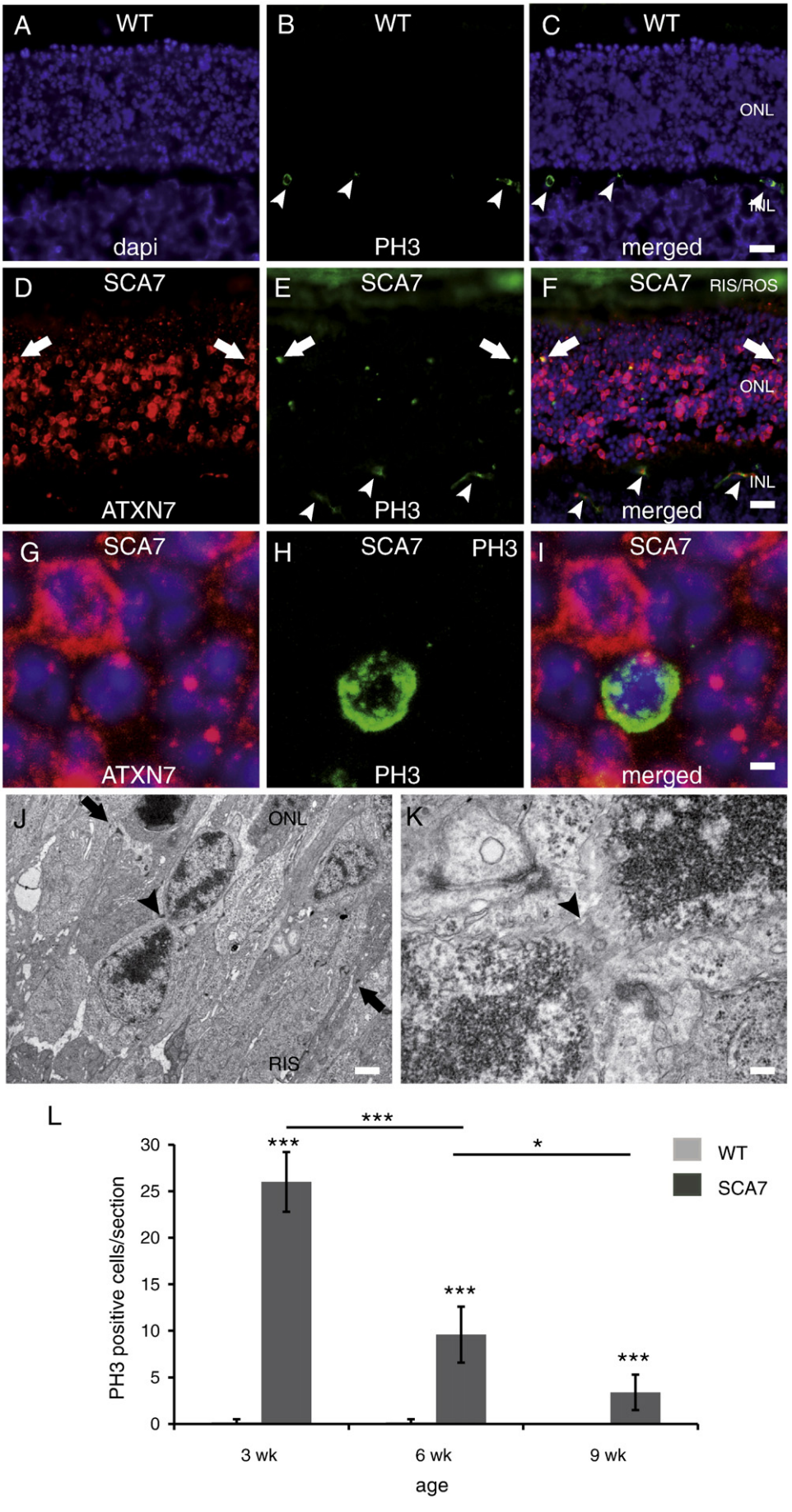
A WT
dapi
B WT
PH3
C WT
ONL
INL
merged
D SCA7
ATXN7
E SCA7
PH3
F SCA7 RIS/ROS
ONL
INL
merged
G SCA7
ATXN7
H SCA7 PH3
PH3
I SCA7
merged
J
ONL
RIS
K
L
***
*
***
***
***
WT
SCA7
PH3 positive cells/section
30
25
20
15
10
5
0
3 wk
6 wk
9 wk
age

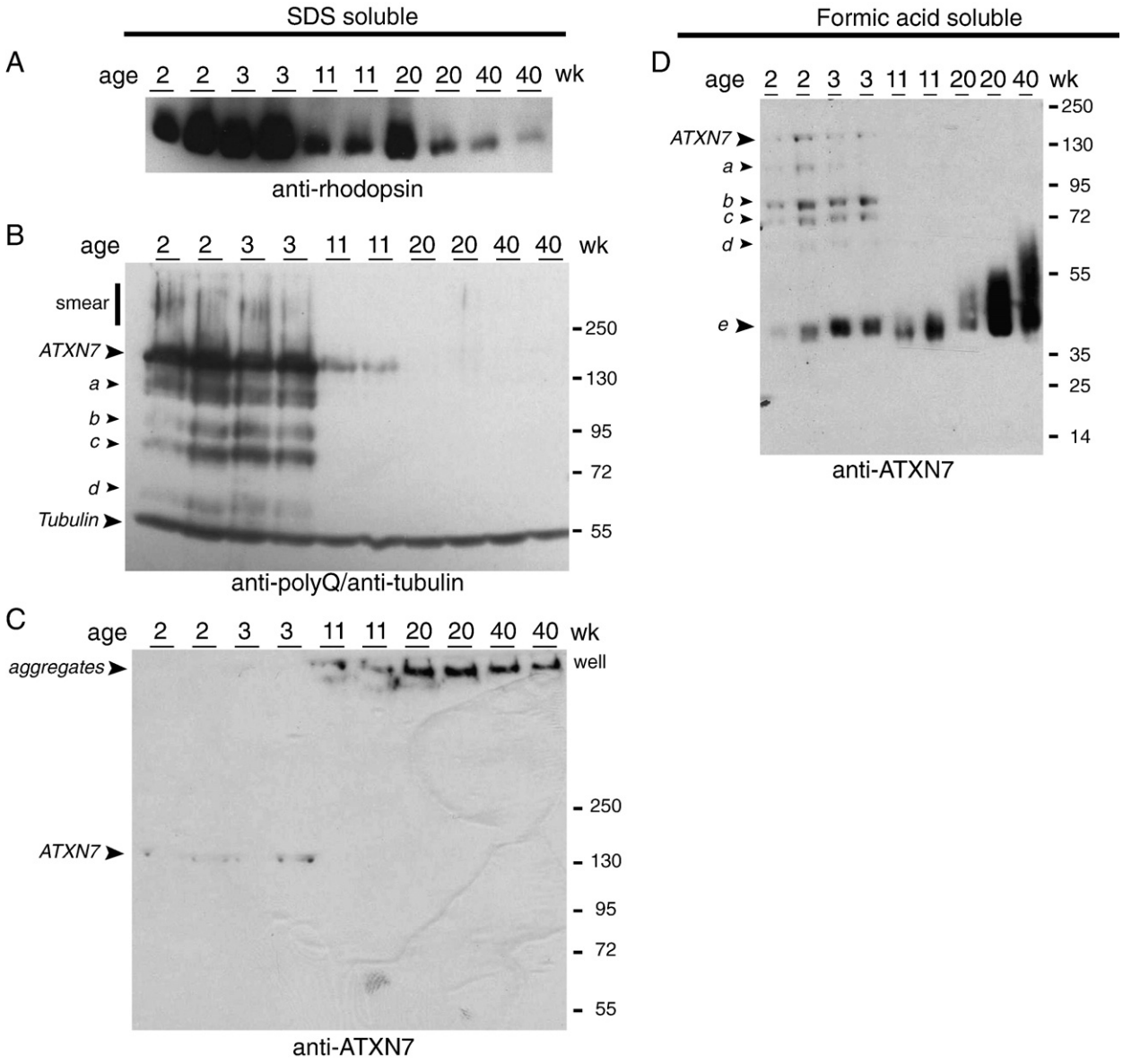

Fig. 9. Different forms of mutant ATXN7 are associated with early and late disease stages. Western blot analysis of SDS soluble (A–C) and formic acid soluble (D) protein extracts of SCA7 retina from PN 2–40wk. (A) Rhodopsin expression progressively decreases from PN 2–3wk to PN 40wk. (B) 1C2 anti-polyQ antibody readily detects full-length mutant ATXN7, proteolytic fragments (a, b, c, d) and a smear at about 250 kDa in the SDS soluble proteins at PN 2–3wk, but not at PN 20–40wk. At PN 11wk, 1C2 reveals only full-length mutant ATXN7, however, at a reduced expression level compared to PN 2–3wk. No ATXN7 product is detected at PN 20wk and 40wk. ß-Tubulin is used as loading control. (C) Anti-ATXN7 antibody detects ATXN7 material in the wells at PN 11wk, 20wk and 40wk, but not at earlier ages (PN 2–3wk). Prior to anti-ATXN7 immunodetection, 1C2 and anti-tubulin antibodies were stripped out of the membrane using standard procedure. However, 1C2 tightly binds to polyQ (Klein et al., 2007) and likely resists to stripping procedure (Y.T., unpublished data). This appears to prevent the detection of full-length mutant ATXN7 and proteolytic fragment by anti-ATXN7 antibody. (D) Anti-ATXN7 antibody detects full-length mutant ATXN7 and proteolytic fragments (a, b, c, d) in the formic acid soluble proteins at PN 2–3wk. An additional ATXN7 fragments (e) is also detected at PN 2–3wk and only this fragment is revealed at PN 11wk, 20wk and 40wk.

stages (PN 2–6wk) is noteworthy as it challenges our current view of neurodegeneration in which we presume that cell death occurs relatively late in the course of degenerative processes.

Although adult neurons are typically described as permanently post-mitotic, there is growing evidence that neurons can re-activate cell cycle conditions in neurodegenerative situations, such as Alzheimer's disease and stroke (for review see Herrup and Yang, 2007). However, in these cases, neurons cannot enter M phase and usually die by apoptosis. Our data suggest that some SCA7 rods divide and go through the entire cell cycle. New SCA7 rods may partially compensate early rod cell death. Cell division is abundant at disease onset, but the frequency decreases with time. Which are these rods that can divide and why cell division decreases as the disease progress? In contrast to inferior vertebrates (Hitchcock et al., 2004), adult neurogenesis seems to be extremely limited in mammalian retina (Menu dit Huart et al., 2004; Moshiri and Reh, 2004). It is also unlikely that deconstructed rods acquire conditions to proliferate, since cell division peaks at PN 3wk, while deconstructed rods are seen later in the disease process. Very recently, it has been shown that upon retinal injury Müller glial cells can transdifferentiate into photoreceptors (Jadhav et al., 2009; Ooto et al., 2004; Wan et al., 2008). Whether Müller transdifferentiation could occur in pathological conditions is unclear. Since signs of mutant ATXN7 toxicity are already visible at the time when the retina still develops (PN 2–3wk), some retinal progenitor cells may proliferate beyond the retinogenesis period to produce lately born rod photoreceptors. Whatever the mechanism, factors permitting the cell cycle entrance and production of new rod cells would be gradually loss with the disease progression.

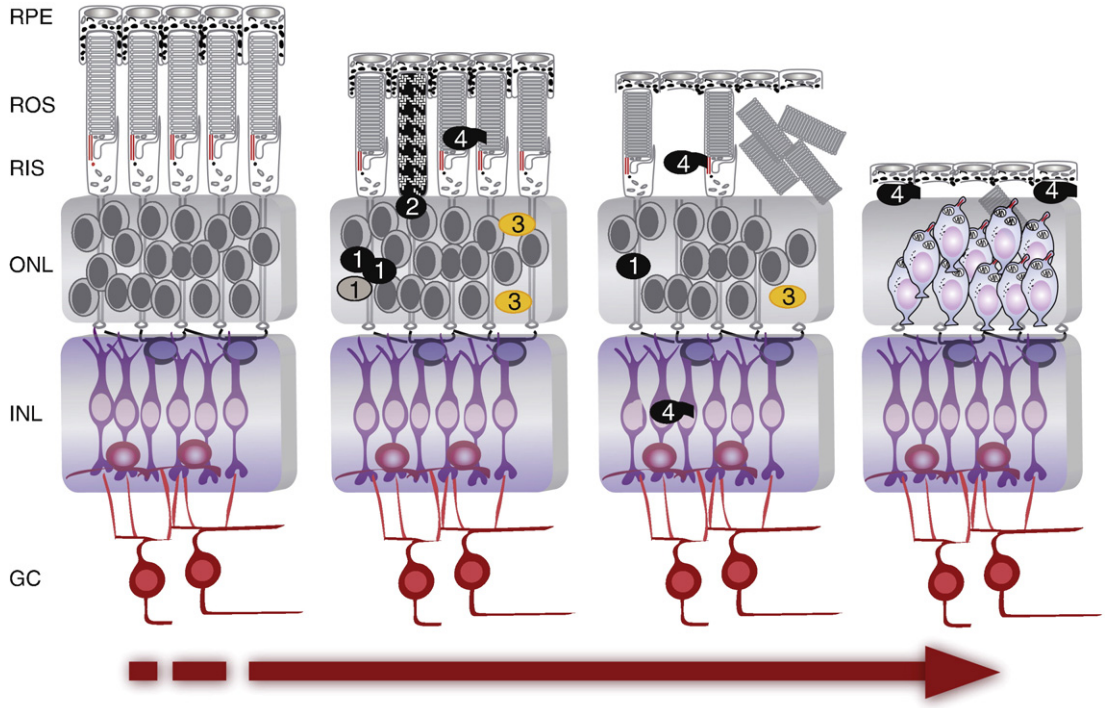

Fig. 10. Complex rod photoreceptor remodeling in SCA7 mouse. SCA7 rod photoreceptors go through a wide range of different cell fates during the time-course of pathological process. Degenerative and regenerative events are the most frequent at early disease stages (2–4th postnatal weeks, second panel from left). At this time point the population of apoptotic (1) photoreceptors is important throughout ONL thickness. Non-apoptotic darkly stained photoreceptors (2) are also present proximally to the segment layer. Both degenerating and living photoreceptors present shortened outer segment in comparison to control retina (left panel). Cell division gives rise to newborn photoreceptor cells (3) and may compensate cell loss in the ONL. The occurrence of apoptosis (1) and cell division (3) declines considerably with disease progression (6–9th postnatal weeks, third panel from left), however rod cell migration (4) increases. Migrating rods are darkly stained and die via non-apoptotic mechanism in both inner retina and segment layer. The subretinal space is filled with degenerating rod outer segment, probably cut off from inner segment at the level of their connecting cilium. Photoreceptor migration (4) remains frequent at the late stages of disease progression (39–42nd postnatal weeks, fourth panel from left). By this time point, surviving photoreceptors display a spherical cell shape with nuclear chromatin decondensation and perinuclear cytoplasm. Surviving photoreceptors result from deconstruction of mature rods and are not anymore functional. Surviving photoreceptors might also originate from rod proliferation.

Whether rods arising from cell division differentiate, remain immature or die, is also a fascinating question to address in the future. The SCA7 mouse retina thus offers a unique opportunity to explore endogenous regenerative potential of rods in adult mammalian retina in degenerative disease situation.

It is noteworthy that in Huntington's disease adult neurogenesis is activated in the subventricular zone near the striatum, the primarily degenerative tissue in this pathology (Curtis et al., 2003). It is tempting to speculate that activation of neurogenesis is a common response to polyQ toxicity. Interestingly, treatments that stimulate neurogenesis improve the neurological phenotype of HD mouse model (Cho et al., 2007; Jin et al., 2005; Peng et al., 2008).

Thus, SCA7 rods go through a wide range of cell fate in response to ATXN7 toxicity. The temporal profile of retinal remodeling indicates that some processes (apoptosis and cell division) are triggered early but decline with the disease course, while others (migration, non-apoptotic cell death, deconstruction) progress slowly (Fig. 10). Although we cannot exclude that some processes interplay, many of them seem to be independently triggered by polyQ toxicity. The results also suggest that a balance between photoreceptors proceeding through death prone versus survival prone (proliferation and deconstruction) pathways could explain the maintenance of the photoreceptor cell population until late disease stage, while retina is non-functional.

PolyQ toxicity: A unique trigger and a wide range of neuronal response

PolyQ toxicity is believed to trigger a cascade of successive degenerative events leading to neuronal death (Finkbeiner et al., 2006; MacDonald et al., 2003). We provide evidence that this view is oversimplified and that *in vivo* neuronal response to polyQ toxicity can be multifaceted. How can a unique toxic protein elicit such a wide range of response in a single neuronal cell type? We show that the pattern of ATXN7 species in the retina largely differs from early to late disease stages. Apoptosis and cell division occurring at early disease stages correlate with the presence of full-length and several proteolytic fragments of mutant ATXN7 in soluble and insoluble forms. In contrast, cell migration, dark degeneration and rod deconstruction, which progressed with the disease and culminated at late stages, are associated with the presence of a unique insoluble fragment of mutant ATXN7. This fragment highly accumulated at PN 20–40wk, despite reduced expression of the mutant ATXN7 transgene (Helmlinger et al., 2004). Our results suggest that the nature, level and ratio of potentially toxic ATXN7 species, which vary considerably from early to late disease stages, influence the way individual neurons respond to proteotoxic stress. These observations may have tremendous importance to design therapeutic strategies for polyQ expansion disorders.

The molecular pathways underlying individual rod responses are yet unclear. However, early studies on SCA7 mouse models point to specific mechanisms that could account for photoreceptor deconstruction. First, ATXN7 is a subunit of the SAGA transcriptional co-regulator complex and polyQ-expanded ATXN7 is thought to alter the SAGA function. Dysfunctional SAGA seems to cause hyperacetylation of histones, chromatin decompaction and inactivation of CRX, a key transcription factor involved in photoreceptor differentiation, leading in turn to down-regulation of photoreceptor gene expression (Helmlinger et al., 2006; La Spada et al., 2001). Second, mutant ATXN7 aggregation activates the Jnk/c-Jun signaling pathway (Merienne et al., 2003), which can repress NRL, a second key transcription factor

regulating photoreceptor differentiation. Blocking c-jun activation delays the retinopathy in the SCA7 model (Merienne et al., 2007). Third, STAT3 signaling pathway is also specifically activated in SCA7 retina. In rodent retina, CNTF treatment also led to STAT3 activation (Rhee et al., 2007). Therefore, STAT3 activation represents a converging pathway in SCA7 and CNTF-treated retinitis pigmentosa models (Beltran et al., 2007; Bok et al., 2002; Liang et al., 2001; Rhee et al., 2007), all showing prominent rod photoreceptor remodeling.

In conclusion, our results revisit the current understanding of how neuronal cells respond to toxic degenerative stresses. The multifaceted response of retinal neurons to polyQ toxicity is as such a new concept that should be taken into account for the design or improvement of therapeutic strategies for polyQ expansion disorders. Moreover, proliferation and protective deconstruction reported in this study underline the high plasticity of rod photoreceptors in response to toxic stress and raises the fascinating question whether these rods can re-differentiate and be functional.

Acknowledgments

We are very grateful to Y. Courtois for careful reading and discussion. We thank J.L. Mandel, K. Mérienne, F. Klein, A. Torriglia, N. Keller, and M. Roux for helpful discussions; N. Daigle for critical reading of the manuscript; C. Bernard for technical assistance; J.L. Vonesh, Y. Lutz and the IGBMC imaging centre. This work was supported by funds from the Centre National de la Recherche Scientifique (CNRS); Institut National de la Santé et de la Recherche Médicale (INSERM); Deutsche Forschungsgemeinschaft [DFG Wo548 to U.W.]; Université de Strasbourg (UdS); European integrated project EUROSCA [LSHM-CT-2004-503304 to Y.T.]. A.K. is supported by a fellowship from Association Connaître les syndromes Cérébelleux.

Appendix A. Supplementary data

Supplementary data associated with this article can be found, in the online version, at doi:10.1016/j.nbd.2010.06.005.

References

Abou-Sleymane, G., et al., 2006. Polyglutamine expansion causes neurodegeneration by altering the neuronal differentiation program. Hum. Mol. Genet. 15, 691–703.
Beltran, W.A., et al., 2007. Intravitreal injection of ciliary neurotrophic factor (CNTF) causes peripheral remodeling and does not prevent photoreceptor loss in canine RPGR mutant retina. Exp. Eye Res. 84, 753–771.
Bok, D., et al., 2002. Effects of adeno-associated virus-vectored ciliary neurotrophic factor on retinal structure and function in mice with a P216L rds/peripherin mutation. Exp. Eye Res. 74, 719–735.
Cho, S.R., et al., 2007. Induction of neostriatal neurogenesis slows disease progression in a transgenic murine model of Huntington disease. J. Clin. Invest. 117, 2889–2902.
Curtis, M.A., et al., 2003. Increased cell proliferation and neurogenesis in the adult human Huntington's disease brain. Proc. Nat. Acad. Sci. U.S.A. 100, 9023–9027.
Custer, S.K., et al., 2006. Bergmann glia expression of polyglutamine-expanded ataxin-7 produces neurodegeneration by impairing glutamate transport. Nat. Neurosci. 9, 1302–1311.
David, G., et al., 1997. Cloning of the SCA7 gene reveals a highly unstable CAG repeat expansion. Nat. Genet. 17, 65–70.
Finkbeiner, S., et al., 2006. Disease-modifying pathways in neurodegeneration. J. Neurosci. 26, 10349–10357.
Fischer, A.J., Reh, T.A., 2001. Muller glia are a potential source of neural regeneration in the postnatal chicken retina. Nat. Neurosci. 4, 247–252.
Fisher, S.K., et al., 2005. Cellular remodeling in mammalian retina: results from studies of experimental retinal detachment. Prog. Retin. Eye Res. 24, 395–431.
Giessl, A., et al., 2004. Differential expression and interaction with the visual G-protein transducin of centrin isoforms in mammalian photoreceptor cells. J. Biol. Chem. 279, 51472–51481.
Gray, M., et al., 2008. Full-length human mutant huntingtin with a stable polyglutamine repeat can elicit progressive and selective neuropathogenesis in BACHD mice. J. Neurosci. 28, 6182–6195.
Helmlinger, D., et al., 2004. Disease progression despite early loss of polyglutamine protein expression in SCA7 mouse model. J. Neurosci. 24, 1881–1887.
Helmlinger, D., et al., 2006. Glutamine-expanded ataxin-7 alters TFTC/STAGA recruitment and chromatin structure leading to photoreceptor dysfunction. PLoS Biol. 4, e67.
Hendzel, M.J., et al., 1997. Mitosis-specific phosphorylation of histone H3 initiates primarily within pericentromeric heterochromatin during G2 and spreads in an ordered fashion coincident with mitotic chromosome condensation. Chromosoma 106, 348–360.
Herrup, K., Yang, Y., 2007. Cell cycle regulation in the postmitotic neuron: oxymoron or new biology? Nat. Rev. Neurosci. 8, 368–378.
Hitchcock, P., et al., 2004. Persistent and injury-induced neurogenesis in the vertebrate retina. Prog. Retin. Eye Res. 23, 183–194.
Jadhav, A.P., et al., 2009. Development and neurogenic potential of Muller glial cells in the vertebrate retina. Prog. Retin. Eye Res. 28, 249–262.
Jin, K., et al., 2005. FGF-2 promotes neurogenesis and neuroprotection and prolongs survival in a transgenic mouse model of Huntington's disease. Proc. Nat. Acad. Sci. U.S.A. 102, 18189–18194.
Jones, B.W., et al., 2003. Retinal remodeling triggered by photoreceptor degenerations. J. Comp. Neurol. 464, 1–16.
Jortner, B.S., 2006. The return of the dark neuron. A histological artifact complicating contemporary neurotoxicologic evaluation. Neurotoxicology 27, 628–634.
Klein, F.A., et al., 2007. Pathogenic and non-pathogenic polyglutamine tracts have similar structural properties: towards a length-dependent toxicity gradient. J. Mol. Biol. 371, 235–244.
Kovesdi, E., et al., 2007. The fate of "dark" neurons produced by transient focal cerebral ischemia in a non-necrotic and non-excitotoxic environment: neurobiological aspects. Brain Res. 1147, 272–283.
La Spada, A.R., et al., 2001. Polyglutamine-expanded ataxin-7 antagonizes CRX function and induces cone-rod dystrophy in a mouse model of SCA7. Neuron 31, 913–927.
Liang, F.Q., et al., 2001. Long-term protection of retinal structure but not function using RAAV.CNTF in animal models of retinitis pigmentosa. Mol. Ther. 4, 461–472.
Lin, B., et al., 2009. Remodeling of cone photoreceptor cells after rod degeneration in rd mice. Exp. Eye Res. 88, 589–599.
Lohr, H.R., et al., 2006. Multiple, parallel cellular suicide mechanisms participate in photoreceptor cell death. Exp. Eye Res. 83, 380–389.
Lunkes, A., et al., 2002. Proteases acting on mutant huntingtin generate cleaved products that differentially build up cytoplasmic and nuclear inclusions. Mol. Cell 10, 259–269.
MacDonald, M.E., et al., 2003. Huntington's disease. Neuromolecular Med. 4, 7–20.
Marc, R.E., et al., 2003. Neural remodeling in retinal degeneration. Prog. Retin. Eye Res. 22, 607–655.
Marc, R.E., et al., 2008. Extreme retinal remodeling triggered by light damage: implications for age related macular degeneration. Mol. Vis. 14, 782–806.
Menu dit Huart, L., et al., 2004. DNA repair in the degenerating mouse retina. Mol. Cell Neurosci. 26, 441–449.
Merienne, K., et al., 2003. Polyglutamine expansion induces a protein-damaging stress connecting heat shock protein 70 to the JNK pathway. J. Biol. Chem. 278, 16957–16967.
Merienne, K., et al., 2007. Preventing polyglutamine-induced activation of c-Jun delays neuronal dysfunction in a mouse model of SCA7 retinopathy. Neurobiol. Dis. 25, 571–581.
Michalik, A., et al., 2004. Spinocerebellar ataxia type 7 associated with pigmentary retinal dystrophy. Eur. J. Hum. Genet. 12, 2–15.
Moshiri, A., Reh, T.A., 2004. Persistent progenitors at the retinal margin of ptc+/− mice. J. Neurosci. 24, 229–237.
Ooto, S., et al., 2004. Potential for neural regeneration after neurotoxic injury in the adult mammalian retina. Proc. Nat. Acad. Sci. U.S.A. 101, 13654–13659.
Peng, Q., et al., 2008. The antidepressant sertraline improves the phenotype, promotes neurogenesis and increases BDNF levels in the R6/2 Huntington's disease mouse model. Exp. Neurol. 210, 154–163.
Pittler, S.J., Baehr, W., 1991. Identification of a nonsense mutation in the rod photoreceptor cGMP phosphodiesterase beta-subunit gene of the rd mouse. Proc. Nat. Acad. Sci. U.S.A. 88, 8322–8326.
Rhee, K.D., et al., 2007. Molecular and cellular alterations induced by sustained expression of ciliary neurotrophic factor in a mouse model of retinitis pigmentosa. Invest. Ophthalmol. Vis. Sci. 48, 1389–1400.
Travis, G.H., et al., 1992. Complete rescue of photoreceptor dysplasia and degeneration in transgenic retinal degeneration slow (rds) mice. Neuron 9, 113–119.
Treisman, J.E., et al., 1988. Opsin expression in the rat retina is developmentally regulated by transcriptional activation. Mol. Cell Biol. 8, 1570–1579.
Trojan, P., et al., 2008. Centrins in retinal photoreceptor cells: regulators in the connecting cilium. Prog. Retin. Eye Res. 27, 237–259.
Turmaine, M., et al., 2000. Nonapoptotic neurodegeneration in a transgenic mouse model of Huntington's disease. Proc. Nat. Acad. Sci. U.S.A. 97, 8093–8097.
Vecino, E., et al., 2004. Cell death in the developing vertebrate retina. Int. J. Dev. Biol. 48, 965–974.
Wan, J., et al., 2008. Preferential regeneration of photoreceptor from Muller glia after retinal degeneration in adult rat. Vision Res. 48, 223–234.
Williams, A.J., Paulson, H.L., 2008. Polyglutamine neurodegeneration: protein misfolding revisited. Trends Neurosci. 31, 521–528.
Yoo, S.Y., et al., 2003. SCA7 knockin mice model human SCA7 and reveal gradual accumulation of mutant ataxin-7 in neurons and abnormalities in short-term plasticity. Neuron 37, 383–401.
Yvert, G., et al., 2000. Expanded polyglutamines induce neurodegeneration and trans-neuronal alterations in cerebellum and retina of SCA7 transgenic mice. Hum. Mol. Genet. 9, 2491–2506.
Zoghbi, H.Y., Orr, H.T., 2000. Glutamine repeats and neurodegeneration. Annu. Rev. Neurosci. 23, 217–247.